J. Fluid Mech. (2017), *vol.* 813, *pp.* 110–126.
doi:10.1017/jfm.2016.849

On the mechanism of high-incidence lift generation for steadily translating low-aspect-ratio wings

Adam C. DeVoria[1] **and Kamran Mohseni**[1,2,†]

[1]Department of Mechanical and Aerospace Engineering, University of Florida, Gainesville, FL 32611, USA

[2]Department of Electrical and Computer Engineering, University of Florida, Gainesville, FL 32611, USA

(Received 19 July 2016; revised 5 December 2016; accepted 5 December 2016; first published online 17 January 2017)

High-incidence lift generation via flow reattachment is studied. Different reattachment mechanisms are distinguished, with dynamic manoeuvres and tip vortex downwash being separate mechanisms. We focus on the latter mechanism, which is strictly available to finite wings, and isolate it by considering steadily translating wings. The tip vortex downwash provides a smoother merging of the flow at the trailing edge, thus assisting in establishing a Kutta condition there. This decreases the strength/amount of vorticity shed from the trailing edge, and in turn maintains an effective bound circulation resulting in continued lift generation at high angles of attack. Just below the static lift-stall angle of attack, strong vorticity is shed at the trailing edge indicating an increasingly intermittent reattachment/detachment of the instantaneous flow at mid-span. Above this incidence, the trailing-edge shear layer increases in strength/size representing a negative contribution to the lift and leads to stall. Lastly, we show that the mean-flow topology is equivalent to a vortex pair regardless of the particular physical flow configuration.

Key words: aerodynamics, separated flows, vortex flows

1. Introduction

Low-aspect-ratio ($\mathcal{R}$) wings have been used for aircraft designs seeking to provide high manoeuvrability, including high-speed fighter jets as well as low-speed, small-scale unmanned aerial vehicles. The flow around a finite-aspect-ratio wing is inherently three-dimensional and thus contains fundamental differences from the much-studied high-aspect-ratio or two-dimensional wings of classical aerodynamics. In this paper, we focus on the mechanism of high lift generation via reattached flow. Early methods aiming to obtain continued lift generation attempted to prevent or delay flow separation completely, such as boundary-layer energization, slotted wings and Prandtl's pioneering work with movement of and suction at the solid surface (see e.g. Goldstein 1938). However, some wings have the ability to allow for

†Email address for correspondence: mohseni@ufl.edu

reattached flow at high incidences. It is theoretically possible to attain reattachment on an infinite-aspect-ratio wing (i.e. two-dimensional flow). In a well-known paper, Saffman & Sheffield (1977) analytically computed the inviscid potential flow around a flat-plate airfoil with a standing point vortex representing the leading-edge separation bubble. They showed that, in principle, it is possible for the vortex to increase the lift significantly above the classical result. In related works, Saffman & Tanveer (1984*a*,*b*) investigated the effects of adding flaps of various orientations at the leading and trailing edges of the wing to assist the separation and reattachment. While they showed similar increases in the lift, solutions were found only for particular arrangements of the flaps and they comment that these constraints may explain the poor performance of previous experimental tests employing such wings.

In the truly steady potential flows discussed above, the reattachment mechanism is the explicit introduction of vorticity into the flow, represented by a stationary point vortex or a vortex sheet coincident with a streamline separating a region of uniform or zero vorticity. However, as demonstrated by Saffman & Tanveer, the ability to establish reattachment can be limited. A more effective mechanism of reattachment is an airfoil/wing that performs a dynamic manoeuvre. This mechanism is associated with generating and delivering large amounts of vorticity into a coherent leading-edge vortex (LEV). The problem of course becomes unsteady, which complicates analysis, but reattachment may occur instantaneously or over some period of time, which is usually related to the time scale of vortex formation, most notably the LEV. The vortex structures created by these time-dependent manoeuvres are known to have significant effects on the instantaneous forces through a phenomena related to 'dynamic stall' (see e.g. McCroskey 1982).

An attached LEV is of major interest in many biologically inspired flows (e.g. Lighthill 1973; Weis-Fogh 1973; Maxworthy 1979; Dickinson & Gotz 1993; Ellington *et al.* 1996; Pitt Ford & Babinsky 2013; Xia & Mohseni 2013) with flapping and rotating wings at large incidences, since the LEV generates much increased lift. Similarly related is research aiming to develop small-scale, low-speed, low-$\mathcal{R}$ microaerial vehicles (MAVs) that are remotely controlled or even autonomous. In this regard, many researchers have studied several canonical manoeuvres for two-dimensional and finite-$\mathcal{R}$ wings, such as pitching (Eldredge, Wang & Ol 2009; Ol *et al.* 2009; Yilmaz & Rockwell 2012), oscillating (McCroskey 1982; Koochesfahani 1989), heaving (Visbal, Yilmaz & Rockwell 2013), plunging (Rival *et al.* 2014), surging (Mancini *et al.* 2015), rotating/revolving (Garmann & Visbal 2014; Wojcik & Buccholz 2014; Carr, DeVoria & Ringuette 2015) and combinations thereof (e.g. Xia & Mohseni 2016). The unsteady aerodynamic loads, most especially the lift, during these manoeuvres have been the focus of such investigations along with dependence on various parameters such as Reynolds number, aspect ratio, reduced frequency, translational and rotational accelerations and radius of gyration to name a few. Also, the dynamic behaviour of the LEV has been of particular interest. More specifically, its circulation growth rate, position/movement relative to the wing and shedding/detachment or lift-off characteristics and how these affect the instantaneous lift. Note that the references listed above represent only a small fraction of the work in this area. However, Bernal (2016) and Ol & Babinsky (2016) provide summaries of some recent work and findings that have resulted from many research efforts. Interestingly, one of the main results is that wings of different geometries and performing different types of manoeuvres display similar lift histories, which is due to similar LEV dynamics in each case.

As mentioned above, dynamic manoeuvres are a rather effective mechanism for generating high lift due to time-dependent reattachment associated with the LEV. It is

by this particular mechanism that larger aspect ratio wings, even two-dimensional airfoils, are able to establish an attached LEV for some amount of time, and thus enjoy increased lift. For these reasons, the study of dynamic wing manoeuvres and their corresponding vortex dynamics have been and remain attractive areas of research, with a surge of publications over the past 20–30 years corresponding to advancements in experimental and computational techniques and capabilities that have improved our understanding of these complex flows.

The present work focuses on the reattachment mechanism for steadily translating low-$\mathcal{R}$ wings, i.e. without dynamic manoeuvres, and so the mechanism is in some sense passive. Obviously the study of these wings is by no means a new subject either. However, there seems to have been less attention paid to the mechanism by which such wings are able to attain reattached flow. This is perhaps because this type of passive reattachment occurs for only very low aspect ratios, namely around unity or below, whereas much of the previous work, including that on the dynamic manoeuvres discussed above, has focused on aspect ratios in the range of $\mathcal{R} = 2$–4 or higher. In fact, for a pitching–flapping wing Jardin, Farcy & David (2012) showed that the tip vortex flow is able to continuously attach the LEV to the wing over a distance of 1.4 chords from the wing tip. They concluded that stable flow cannot be maintained if $\mathcal{R} > 1.4$. For steadily translating wings we suspect that the reason such small aspect ratios are necessary for this passive reattachment mechanism is because the rate at which vorticity is generated is not associated with any type wing acceleration. As such, some other agency is required to organize the presumably weaker vorticity into a useful configuration analogous to a LEV.

For the case of steadily translating wings, the instantaneous flow and forces are still time dependent of course. However, transients associated with initial movements have subsided and the wing has travelled an infinite number of chord lengths. Ol & Babinsky (2016) note that for wings which perform a dynamic manoeuvre into translation, the 'steady-state' lift value is reached after approximately 15 chord lengths of travel, although there still may be some residual transients at this time (Mancini *et al.* 2015). Nonetheless, the vortex dynamics is different from that dominated by the dynamic manoeuvre. Moreover, for a typical fixed-wing MAV flight speed ($\sim$10 m s^{-1}) and mean chord ($\sim$15 cm), approximately 65 chord lengths will be travelled in 1 s; hence short-time steady translation is relevant to the flight envelope. Also, with an operating Reynolds number of $O(10^4$–$10^5)$ the vortex dynamics is not necessarily characteristic of an organized von Kármán vortex street. Given this, and the consideration of very low aspect ratios, the concept of coherent LEVs (paired with trailing-edge vortices) shedding from the wing in a regular or organized manner is not necessarily an appropriate representation of this flow.

Accordingly, the reattachment mechanism is intermittent and is associated with oscillations of the leading-edge shear layer, as well as shedding of vortical structures. As an approximation of the expected oscillation/shedding frequencies, consider the Strouhal number of two-dimensional airfoils reported by Katz (1981), namely $St \approx 0.15$–0.18. For a wing with the typical MAV dimension/flight speed mentioned above and 10° incidence, the frequency is estimated to be $\sim$55–70 Hz. Therefore, in this paper we consider the time-averaged flow of steadily translating low-$\mathcal{R}$ wings and investigate how changes of the aspect ratio and incidence affect the mean-flow reattachment. Also, while the time-averaged flow does show a generally recirculating region (see figure 3), the centre of rotation is not characterized by strong vorticity, which is in contrast to a LEV. For this reason, we instead use the term 'leading-edge separation region' (LESR) to indicate it is a time-averaged result of unsteady structures.

The paper is organized as follows. The experimental set-up is described in § 2. The measurements of the time-averaged flow fields are presented in § 3 and the results discussed from an observational point of view. Then, in § 4 a discussion is given on the postulation that the tip vortex downwash is the reattachment mechanism for steadily translating low-$\mathcal{AR}$ wings. The flow fields are then interpreted through inviscid potential flow concepts in § 5 as well as through topological concepts in § 6.

2. Experimental set-up

Planar digital particle image velocimetry (DPIV) measurements in the mid-span plane of the wings are performed in a recirculating wind tunnel that has a cross-section of 61×61 cm^2, a test section length of 2.44 m. Flat-plate, rectangular wing models of aspect ratios $\mathcal{AR} = 0.75$, 1, 1.5, 2, and 2.5 are investigated (see figure 1*a*); the aspect ratio is conventionally defined as $\mathcal{AR} \equiv b_{max}^2/S = b/c$, where $b_{max} \equiv b$ and c are the rectangular wing span and chord. For each aspect ratio, the angle of attack is varied in 5° increments from 0° to 45°; the angle of attack is set manually to within $\pm 0.1°$ using a digital protractor. The rectangular wings are machined from clear acrylic sheets; the chord is kept constant at $c = 101.6$ mm and the span is varied to change the aspect ratio. The leading and trailing edges were rounded with elliptical profiles of ratios 5 : 1 (blunt) and 20 : 1 (sharp), respectively, while the side edges were left square. For $\mathcal{AR} \leqslant 2$, the plate thickness is 3.175 mm, while for $\mathcal{AR} = 2.5$ the thickness is 4.76 mm, giving thickness ratios of 3.1 % and 4.67 %, respectively. With a free stream velocity of $U = 11.93$ m s^{-1} the chord-based Reynolds number is approximately $Re = 80\,000$.

The main objective of the current experiments is to study the effect of aspect ratio on the flow at the mid-span plane of the wings, and so the wing mounting device (figure 1*a*) is designed to interfere as little as possible with this area. The device consists of two stainless steel rods (6.35 mm dia.) to which the plate is secured via countersunk machine screws. The distance between these holes is 50.4 mm and is centred about the mid-span of the plates; this spacing is the same for all $\mathcal{AR}$ so that the effect of sting on the mid-span flow remains the same. The sting rods may be rotated and extend back to a block housing, which can also rotate via its connection to a steel post through the tunnel ceiling panel. These two pivot points allow the angle of attack to be set while maintaining a relatively fixed position of the plate model in the camera image.

The wind tunnel is seeded with olive oil particles (~ 1 μm). The DPIV system consists of a high-speed CMOS 1 Mpx camera and a 20 mJ Nd : YLF laser. For each $\mathcal{AR}$ and α combination, 400 image pairs are acquired at a frequency of $f_s = 1000$ Hz. As an *a posteriori* check on this relatively short acquisition time of 0.4 s, circulations were computed from mean vorticity fields that were time averaged over an increasingly larger sample time; also computed were the corresponding standard deviations. It was found that major variations subsided by 0.2 s of sample time (i.e. 200 samples). Therefore, this suggests that the 0.4 s acquisition time is sufficient to capture the true time average of the vorticity fields and circulations, which are the main quantities reported in this paper.

Although the instantaneous flow is unsteady, these oscillations have an amplitude whose magnitude is acceptably smaller than that of the time-averaged flow. The inset of figure 1(*b*) plots the time-dependent positive circulation, $\Gamma(t) > 0$, normalized by its mean, $E(\Gamma)$, for a sample case. For this example, the circulation oscillates with amplitude approximately 10 % of the mean. The main plot of figure 1(*b*) shows the

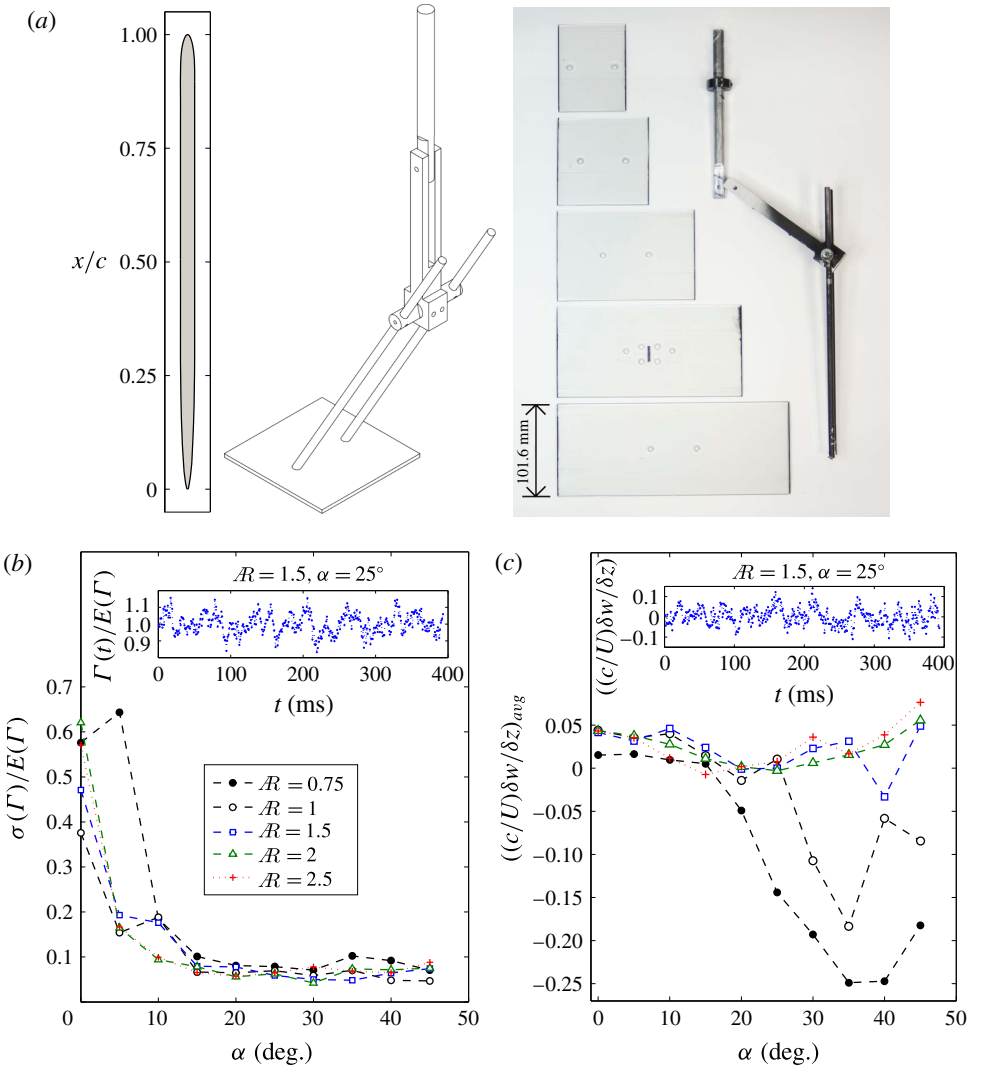

FIGURE 1. (Colour online) (*a*) The wing cross-section, drawing of the mounting device and an image of the actual wings and mounting device. (*b*) The mean-normalized circulation standard deviation, $\sigma(\Gamma)/E(\Gamma)$, for each $\mathcal{AR}$ case. Inset: the time-dependent circulation, $\Gamma(t)$, normalized by $E(\Gamma)$ for a sample case. (*c*) Spatio-temporally averaged out-of-plane strain rate for each $\mathcal{AR}$ case to quantify three-dimensional effects. Inset: the spatial average of this strain rate as a function of time for a sample case.

standard deviation of the circulation, again normalized by the mean, for each $\mathcal{AR}$ case as functions of the angle of attack. At small angles of attack this normalized standard deviation is larger because there is not much vorticity in the flow so that the mean itself is a small number (see figure 5). For $\alpha > 15°$ the oscillation amplitudes for each case are again approximately 10 % of the corresponding mean. The instantaneous flow is also three-dimensional (see e.g. Yilmaz & Rockwell 2012), and we attempt to assess the degree of out-of-plane effects in the two-component, planar measurements. We compute the spatially averaged out-of-plane strain rate,

$\partial w/\partial z = -(\partial u/\partial x + \partial v/\partial y)$, as a function of time. Large fluctuations due to spanwise flows are expected, but we assume that these fluctuate around a near-zero mean and therefore do not much affect the time-averaged two-dimensional flow fields. The inset of figure 1(*c*) shows this spatially averaged strain rate for a sample case, which is just after the static lift-stall angle. The inset shows fluctuations around a near-zero time average of $(\partial w/\partial z)_{avg} \approx 0.0037$. The main plot in figure 1(*c*) shows the $(\partial w/\partial z)_{avg}$ for each $\mathcal{R}$ as functions of angle of attack. For $\mathcal{R} \geqslant 1.5$, there are not drastic changes in the average strain rate over the range of α, but for $\mathcal{R} \leqslant 1$ the three-dimensional effects become increasingly significant. This is not too surprising since any tip vortex wandering (Kaplan, Altman & Ol 2007) could pass into the mid-span plane. However, it is the square of the out-of-plane strain that is relevant to two-dimensionality (DeVoria & Ringuette 2012), so the squared value should be small compared to relevant in-plane strains (e.g. vorticity/circulation), which is acceptably confirmed by the circulations plotted in figure 5.

The DPIV images are processed using an iterative multi-pass DPIV evaluation algorithm with window shifting/deformation. The rectangular interrogation windows start from 64×40 px^2 and go to 32×20 px^2 with 50 % overlap. The spatial resolutions of the DPIV data are then $\Delta x = 0.029c$ and $\Delta y = 0.018c$ in the horizontal and vertical directions, respectively. Measurement uncertainties are obtained by analysing images of the undisturbed free stream velocity and are estimated to be $\delta u/U \approx \delta v/U \approx 0.006$. Using the smallest vector spacing, the uncertainty in the vorticity is $\delta\omega c/U = 0.203$, which is obtained from the 'local circulation method' (Raffel, Willert & Kompenhans 1998).

Forces are measured using a specially designed micro-loading technologies (MLT) six-component internal force balance, which has been validated to measure small aerodynamic loads (Shields & Mohseni 2013). Each model is swept through an angle of attack range from $\alpha = 0$ to 46° in 2° increments. At each α, data acquisition is halted for 4 s to allow for initial flow transients to subside. Each force balance channel is sampled at 4096 Hz and a total of 16 384 samples are acquired. An identical sweep is made beforehand with the wind off, which acts as a tare set. The acquired data are then converted to aerodynamic loads using techniques outlined by the AIAA strain-gauge standard (AIAA Standards 2003). Blockage effects from streamline curvature, wake and solid bodies are corrected for based on methods presented by Rae & Pope (1984). The forces are non-dimensionalized into coefficients using $(\rho U^2 S)/2$ as a normalization.

3. Observed flow description

Before presenting the DPIV measurements, we introduce the lift and drag coefficients, C_L and C_D, in figure 2, which will aid the following discussions in relating changes of the flow character to the global quantities of lift and drag. Note that the static lift stall occurs at lower angles of attack as the aspect ratio increases. More specifically, the $\mathcal{R} = 0.75$, 1, 1.5, 2 and 2.5 wings stall at $\alpha_s \approx 40°$, 35°, 22°, 17° and 12°, respectively. As will be discussed below, this delay in lift stall correlates with decreased shedding of high-magnitude vorticity from the trailing edge.

Note that since the flow fields are time averaged, changes in the angle of attack are regarded as parametric variations and are not to be confused with time-dependent variations that would occur during a dynamic manoeuvre. For $\alpha < 10°$ the time-averaged flow fields for each $\mathcal{R}$ are essentially the same and exhibit attached flow. The velocity field is nearly potential with vorticity being limited to

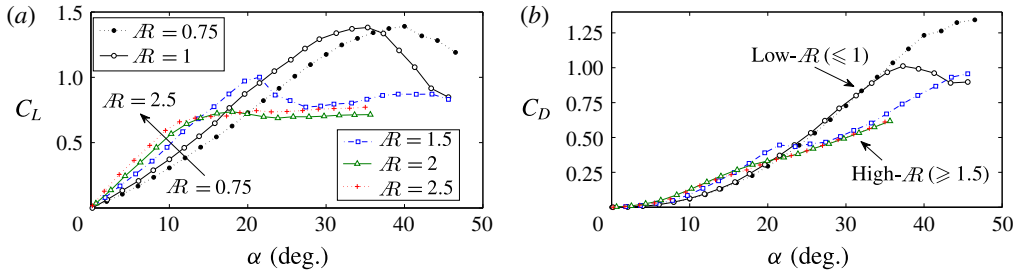

FIGURE 2. (Colour online) Direct force transducer measurements of the (*a*) lift coefficient C_L and (*b*) drag coefficient C_D as a function of angle of attack for $\mathcal{AR} = 0.75$, 1, 1.5, 2 and 2.5.

a boundary-layer-like flow around the wing and shed into a thin wake at the trailing edge. The vorticity can here be described as a region of low total head and without definite separation of the flow from the wing (Goldstein 1938), and as the incidence is increased this region approaches the leading edge. Steady, attached flow is the hallmark of classical aerodynamics and for this reason we do not discuss further the flow characteristics in this regime. Next, an observational discussion is provided on how the flow changes with incidence and aspect ratio.

Figure 3 plots the time-averaged vorticity fields for the cases of $\mathcal{AR} = 0.75$, 1, 1.5, 2 and 2.5 and for $\alpha = 10°$–$40°$. Also shown are the streamlines of the corresponding mean velocity fields. For the $\mathcal{AR} = 0.75$ and 1 wings at $\alpha = 10°$ the mean flow is still attached and maintains a potential-like velocity field with minor shedding of vorticity. For $\mathcal{AR} = 1.5$ the magnitude of shed vorticity has increased, which is related to the boundary-layer instability growing larger in amplitude with intermittent separation, although this separation has not yet reached the leading edge. In the mean sense the flow is still nominally attached and no recirculating zone appears. For $\mathcal{AR} \geqslant 2$ strong shear layers appear close to or at the leading edge and are accompanied by reversed flow near the wing surface. The streamlines for these cases do not indicate a closed separation region. However, this behaviour is explained by examining movies of the instantaneous flow fields for $\mathcal{AR} \geqslant 2$ at $\alpha = 10°$, which show vortices close to the wing surface advecting downstream along a large portion of the chord, but lift off toward the trailing edge. Nonetheless, it can be concluded that decreasing the aspect ratio suppresses the growth of the boundary layer and delays the approach of separation toward the leading edge as α is parametrically increased; this is similar to energizing the boundary layer.

By $\alpha = 15°$ separation occurs at the leading edge for all $\mathcal{AR}$ cases tested, and a separation region exists, which is larger in size with increasing $\mathcal{AR}$. For the purpose of discussion, we assume that the initial formation of the leading-edge shear layer results in a separation region, however small, with a stagnation/reattachment point, say x_r, aft of the leading edge, and that this point approaches the trailing edge as α is increased. Observation of figure 3 shows that the larger the aspect ratio the lower α will be when x_r reaches the trailing edge and results in drastic changes to the flow character, as can be verified by the differences from $\alpha = 10°$ to 15° in the flow fields of the $\mathcal{AR} = 2$ and 2.5 wings. When x_r passes the trailing edge it moves into the fluid and an opposite-sign shear layer is then generated at the trailing edge. The situation when x_r has just passed the trailing edge is approximately seen for the $\mathcal{AR} = 1.5$ wing at $\alpha = 15°$. An increase in α or $\mathcal{AR}$ will exacerbate this situation and the reversed flow

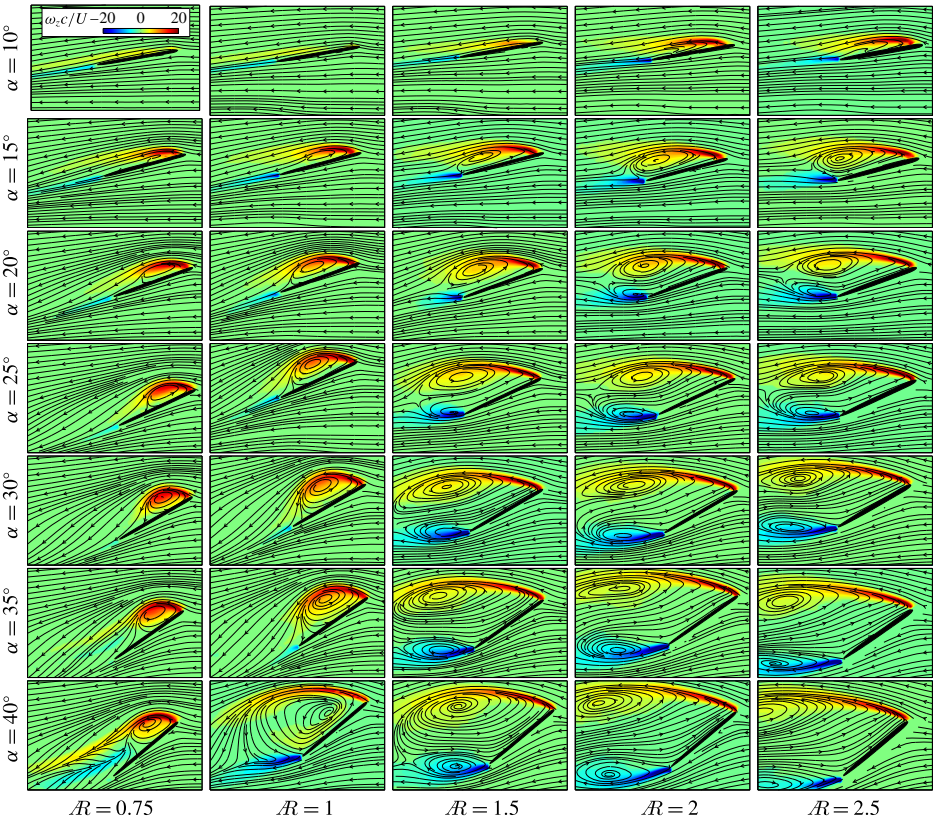

FIGURE 3. Time-averaged non-dimensional vorticity ($\omega c/U$) fields and corresponding streamlines at mid-span for $\mathcal{AR} = 0.75$, 1, 1.5, 2 and 2.5 (left-to-right) and for $\alpha = 10°$–$40°$ (top-to-bottom). The colour bar in top left corner applies to all plots. Gaps apparent in the streamline data near the wing surface are due to the parallax view of the plate in the camera images.

in the separation region becomes increasingly anti-parallel to the pressure side flow, thus increasing the strength of the trailing-edge vorticity. A counter-rotating separation region (CRSR) then forms and x_r is at the rear of the separation region (e.g. $\mathcal{AR} \geqslant 1.5$, $\alpha = 25°$ cases).

The $\mathcal{AR} = 0.75$ and 1 wings are unique in that they maintain reattached flow with a single separation region (i.e. the LESR), and thus continued lift generation, until $\alpha_s \approx 35°$ and 40°, respectively. The peculiar source-like streamlines of the $\mathcal{AR} = 0.75$ case at this high incidence are a result of increased three-dimensionality associated with the wandering of the tip vortices in and out of the mid-span plane (recall figure 1*c*). A counter-rotating separation region is not observed for $\mathcal{AR} = 0.75$ and 1 even at the highest angle of attack tested ($\alpha = 45°$), which is likely related to the tip vortex downwash impeding the roll-up process. However, a CRSR is certain to be present as $\alpha \to 90°$, where the flow (in the time-averaged sense) is similar to bluff body or Prandtl–Batchelor flow (Batchelor 1956; Saffman & Tanveer 1984*a*).

For all aspect ratios, the drag obviously increases with angle of attack since the suction of the vortex flow (for either reattached or fully separated flow) generates a force in the direction of the normal of the wing surface (Polhamus 1966), the

horizontal component of which is $\sin\alpha$. Evidently, the drag penalty is then greater for the low-$\mathcal{AR}$ wings that maintain reattached flow (see figure 2).

Comparing the C_L in figure 2 with the mean-flow fields in figure 3, it can be seen that the static lift stall occurs just after there is an increase of opposite-sign vorticity at the trailing edge. Therefore, the appearance of high-magnitude vorticity shedding at the trailing edge indicates the imminence of lift stall and a change in the flow structure. Reducing the aspect ratio (i.e. closer tip vortices) is seen to suppress the spatial growth of the separation region and to delay the approach of the reattachment point to the trailing edge. In fact, for the low-$\mathcal{AR}$ cases the weak, opposite-sign vorticity near the trailing edge at $\alpha = 15^\circ$ actually decreases and nearly vanishes as α is increased further. Hence, it seems that the growing strength of the tip vortices with α (Clark, Smith & Thompson 1975; Kaplan *et al.* 2007) induces a flow that aids smoother merging of the flows from the suction and pressure sides of the wing at the trailing edge and consequently decreases shedding of strong trailing-edge vorticity.

4. Tip vortex downwash and reattachment

Since decreasing the $\mathcal{AR}$ brings the tip vortices in closer proximity of one another, the reattachment mechanism is often attributed to the momentum provided by their induced downwash (Winter 1936; Jian & Ke-Qin 2004; Taira & Colonius 2009*b*). Similar explanations have been given for LEV attachment in wings performing dynamic manoeuvres, such as flapping wings using translation (Shyy *et al.* 2009; Kim & Gharib 2010; Jardin *et al.* 2012) and rotation (Birch & Dickinson 2001; Ozen & Rockwell 2012). For the steadily translating wings studied here, this reasoning is very probable, however it remains speculative and does not offer further information on the details of the reattachment mechanism or the transition from reattached to fully separated flow as the aspect ratio or incidence is increased. Here, we use the volumetric reconstructions of DeVoria & Mohseni (2015) as well as our current measurements to provide more evidence of the tip vortex downwash as the reattachment mechanism.

DeVoria & Mohseni (2015) measured the three-dimensional flow around $\mathcal{AR} = 1$ and 3 flat-plate, rectangular wings at $\alpha = 35^\circ$ with stereo digital particle image velocimetry. Figure 4 shows contour plots of the downward vertical velocity, $v/U < 0$, for these wings. For $\mathcal{AR} = 1$ the flow is reattached and it is seen that v/U has magnitudes in excess of half the free stream velocity. The plot locations shown are aft of the mid-chord location, where the LESR begins its reattachment (see figure 3), and so the large magnitudes of v/U occur outside this region. This indicates that the tip vortices act mostly to reattach the downstream portion of the leading-edge shear layer onto the plate surface, rather than pinning the whole region to the wing. Conversely, for $\mathcal{AR} = 3$ the flow is fully separated and the contours of v/U are considerably weaker (near zero). More importantly, though, these regions of v/U correspond to the counter-rotating recirculation zone within the massive separation region and are not representative of any tip vortex flow.

One can imagine that the induced flow of the tip vortices has a significant effect on the flow near the trailing edge. Figure 4 also shows iso-surfaces of the negative spanwise vorticity component shed by the two wings, which is almost entirely generated from the trailing edge. For the $\mathcal{AR} = 1$ case the trailing-edge vorticity is quickly wound up around the strong, well-formed tip vortices which are clearly identified or 'tagged' by the rolled up spanwise vorticity. On the other hand, for the $\mathcal{AR} = 3$ case the trailing-edge vorticity extends well into the wake and the tip vortices

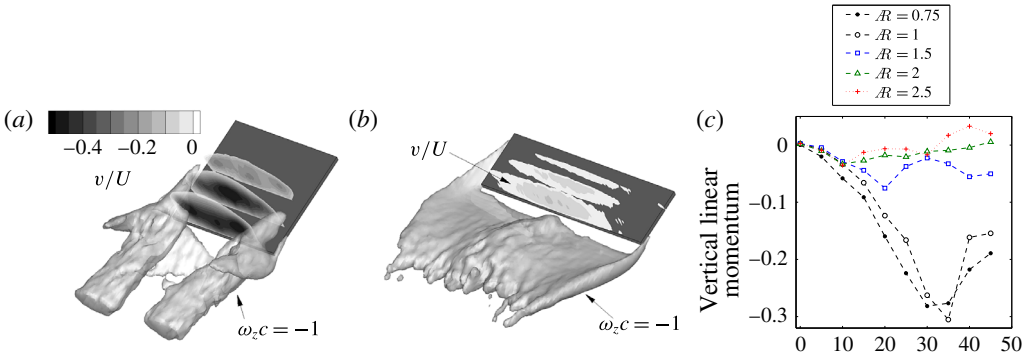

FIGURE 4. (Colour online) Contour plots of the downward vertical velocity $v/U < 0$ at several constant chord locations for (*a*) $\mathcal{AR} = 1$, reattached flow, and (*b*) $\mathcal{AR} = 3$, fully separated flow. Also shown are iso-surfaces of the negative spanwise vorticity shed ($\omega_z c/U = -1$) from the trailing edge. These data are from the experiments of DeVoria & Mohseni (2015) for wings at $\alpha = 35°$ and $Re = 80\,000$. (*c*) Integrated normalized vertical linear momentum versus α for the data from the current paper for each $\mathcal{AR}$.

have less effect on it, as already indicated in the previous paragraph. We reiterate that the trailing-edge vorticity shown in figure 4 corresponds to spanwise vorticity and not a streamwise vortex sheet as is usually described for conventional high-aspect-ratio wings at low incidences (e.g. Prandtl's lifting line theory).

To provide further evidence, we use the data of the current experiments to estimate the total (i.e. integrated) linear momentum of the vertical velocity component, v, within the measurement window. This is computed as $\int \rho v \, \mathrm{d}A$ and is normalized by ρUA, which represents the linear momentum of the free stream integrated over the same measurement plane area A. Also, recall that the chord and free stream speed are the same for each wing and so the only dimensional difference for a given angle of attack is the span. Imparting negative/downward vertical momentum into the fluid is, of course, indicative of lift generation. The right-most plot in figure 4 shows this integrated and normalized vertical linear momentum for each $\mathcal{AR}$ as a function of angle of attack. The lowest aspect ratios ($\mathcal{AR} \leqslant 1$) show higher magnitudes of this momentum and a continued monotonic trend for a larger incidence range. The higher $\mathcal{AR}$s do not continue to impart more downward momentum because either they cannot maintain reattached flow ($\mathcal{AR} = 1.5$) or the flow becomes fully separated at low incidences ($\mathcal{AR} \geqslant 2$, $\alpha \approx 10°$). Trends with similar physical implications are observed in the lift/drag coefficients (recall figure 2) and the mid-span circulation as will be shown in § 5.1.

Based on these quantitative results, it is quite reasonable to assume that for steadily translating low-$\mathcal{AR}$ wings the tip vortex downwash is indeed the mechanism that causes a reattached mean flow provided $\mathcal{AR}$ is sufficiently small, and that this mechanism is seemingly natural or passive.

5. Inviscid flow description

In this section, we interpret the observations of § 3 in a manner that is consistent with inviscid, potential flow concepts. For this purpose, we first regard the mean flow in the mid-span plane as two-dimensional with the three-dimensional effects of a finite aspect ratio and the tip vortex flow represented as some external agency

that can alter the flow character. First, recall that potential flow theory allows a solid body in a uniform flow to be represented by the closed streamline corresponding to the complex potential obtained from the superposition of the potentials for a vortex doublet (or source doublet) and a plane flow. The Kutta condition is then imposed by the development of the bound circulation Γ_b around the wing, with the Helmholtz law of persistence of irrotationality being satisfied by the 'starting vortex' of equal and opposite circulation Γ_s located at an infinite distance downstream.

Consider attached flow and allow the wing to move impulsively from rest to its steady translation speed. The bound circulation will build up to the magnitude of the starting vortex. The effect of the starting vortex on the build-up of Γ_b is often referred to as the Wagner effect. For finite-$\mathcal{R}$ wings, the induced velocity of the tip vortex flow results in a similar effect. However, since the tip vortices move with the wing, this effect is omnipresent meaning that the steady-state bound circulation value for a low-$\mathcal{R}$ wing is less and consequently less lift is generated as compared to a higher-$\mathcal{R}$ wing at the same angle of attack in the attached flow regime (see figure 2). This is, of course, consistent with the effective angle of attack concept associated with lifting line theory and which also results in reduced lift.

Now, at some angle of attack the bound circulation will be too large to remain completely bound to the wing. Physically, this corresponds to separation and a leading-edge vortex sheet is released into the fluid. In the case of reattached flow, a single LESR forms and has a rotation that is of the same sense as the bound circulation. The irrotational flow is now that around the closed streamline of the LESR (similar to Saffman and coworkers), and around which there is an effective bound circulation that includes the vortex sheet strength, say Γ_{le}. Furthermore, the vortex sheet must have an 'image system' inside the wing in order to satisfy the no-flow-through condition. The Helmholtz law becomes

$$(\Gamma_b + \Gamma_{le}) - \Gamma_s = 0. \tag{5.1}$$

Here, the reattachment point x_r exists on the wing and thus the flow over the trailing edge is able to merge smoothly with the flow coming from the pressure side, thus establishing a Kutta condition at the trailing edge. So long as the flow stays reattached, the effective bound circulation, $\Gamma_o = \Gamma_b + \Gamma_{le}$, results in lift enhancement.

Similar to the way in which the bound circulation cannot grow indefinitely in a real viscous fluid, so too must the effective bound circulation of the reattached flow be limited. Stated differently, as the angle of attack and/or $\mathcal{R}$ increases the image system of the leading-edge vortex sheet will, at some point, no longer be able to stay confined inside the wing. The 'excess' image vorticity is then released into the flow via shedding of an opposite-sign vortex sheet at the trailing edge. This occurs when the reattachment point reaches the trailing edge (recall the discussions of § 3). Representing the trailing-edge vortex sheet by Γ_{te}, the Helmholtz law now yields

$$(\Gamma_b + \Gamma_{le} - \Gamma_{te}) - \Gamma_s = 0. \tag{5.2}$$

The trailing-edge vortex sheet contribution, $-\Gamma_{te}$, to the effective bound circulation, $\Gamma_o = \Gamma_b + \Gamma_{le} - \Gamma_{te}$, thus results in a negative contribution to the lift. The argument that lift loss occurs when x_r passes the trailing edge garners support from the solutions given by Saffman & Sheffield (1977) for a standing point vortex over a wing. They enforced the condition that the (finite) trailing-edge velocity tangential to the wing be in the downstream direction. It was found that maximum lift occurs when the trailing edge is a stagnation point, i.e. when x_r exists there. More solutions exist,

but which violate the imposed condition meaning that there is reversed flow over the trailing edge. This reversed flow is exactly the situation described in § 3 that creates trailing-edge vorticity and leads to lift stall. Hence, in the context of the potential solutions, an opposite-sign point vortex, namely $-\Gamma_{te}$, should be introduced to represent the different physics. More concrete, experimental evidence of lift loss coinciding with x_r reaching the trailing edge was shown by Rival *et al.* (2014), where the instantaneous lift of a plunging two-dimensional profile dropped rapidly as the LEV detachment process progressed. We also further quantify and discuss this concept with our experimental measurements of circulation in § 5.1.

It is also interesting to comment on the starting vortex as a source of the image system vorticity. If we let the single separation region be represented by a free vortex Γ_{le}, then the image system consists of a same-sign vortex Γ_{le} at the origin and an opposite-sign vortex $-\Gamma_{le}$ at the inverse point inside the cylinder. The bound circulation is also located at the origin. Hence, with (5.1) the vortices at the origin could be thought of as the mirror image of the starting vortex, which is located at infinity. The image system is then decomposed into the mirror images of the starting vortex and the free vortex. When the trailing-edge vortex sheet is shed, (5.2) indicates that Γ_s will decrease as the trailing-edge vorticity lowers the effective bound circulation of the counter-rotating separation region. Recognizing that the Joukowski transformation maps the point at infinity in the physical plane to the origin of the virtual circle plane, we can then view this decrease of Γ_s as circulation returning to the wing, which then exits again at the trailing edge. Accordingly, at very high angles of attack the CRSR becomes more symmetrical and Γ_s continually decreases. Then as $\alpha \to 90°$ no starting vortex is shed, $\Gamma_s = 0$, and assuming symmetry of the flow then $\Gamma_{le} = \Gamma_{te}$ and so $\Gamma_b = 0$.

5.1. *Experimental circulation*

Here, we use the measurements to quantitatively validate the statements made previously about the loss of lift occurring when the reattachment point passes the trailing edge and vorticity is generated there. Again, Rival *et al.* (2014) observed this to be the case for a dynamic manoeuvre of two-dimensional wings. With the experimental data we cannot distinguish a bound circulation, however the positive and negative contributions to the total circulation can be measured. For simplicity, let the regions of total positive and negative vorticity in the flow be represented by separate circulation magnitudes: Γ^+ and Γ^-, respectively. Then, the Joukowski lift formula gives:

$$L = \rho U(\Gamma^+ - \Gamma^-). \tag{5.3}$$

When there is no separation Γ^+ is essentially the bound circulation of classical steady aerodynamics. For separated, but reattached flow $\Gamma^+ \gg \Gamma^-$ and the lift is enhanced for a given $\mathcal{AR}$ by the separation region. Finally, for fully separated flow the strength of the trailing-edge vorticity increases significantly as discussed previously and if the increase of Γ^+ with a corresponding increase of α is less, then the lift will decrease. Figure 5 plots the non-dimensional experimental Γ^+ and Γ^- as functions of α for the different aspect ratios. The circulations are computed from the (discrete) area integral of vorticity of the positive and negative vorticity fields, which are thresholded above the measurement uncertainty level to avoid accumulation of low-level vorticity in the result. It is seen that Γ^+ generally grows with α and shows a marked increase when the leading-edge shear layer forms ($\alpha \approx 5$–$10°$). For $\mathcal{AR} \geqslant 1.5$, the same is true for Γ^-. However, for $\mathcal{AR} \leqslant 1$, Γ^- is seen to decrease in magnitude after the formation of the

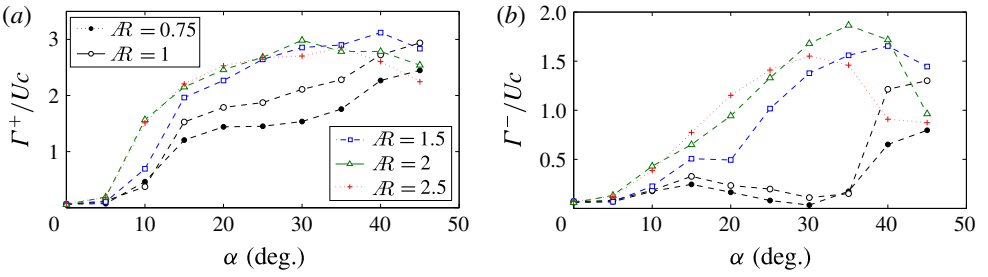

FIGURE 5. (Colour online) The measured non-dimensional circulation magnitudes associated with (*a*) positive vorticity Γ^+/Uc, and (*b*) negative vorticity Γ^-/Uc as a function of angle of attack for each aspect ratio. Note that at the largest values of α the vorticity field of a few $\mathcal{AR}$ cases is not entirely contained within the measurement plane (figure 3). However, the missing vorticity is of low magnitude.

leading-edge shear layer, which explains why the decrease of trailing-edge vorticity via tip vortex downwash for low-$\mathcal{AR}$ wings results in continued lift generation at large angles of attack.

In fact, Taira & Colonius (2009*a*) found that flow control via downstream blowing along the trailing edge was most effective in maintaining increased lift at larger incidences for low-$\mathcal{AR}$ wings at $Re = 300$. They concluded that the downstream blowing at the trailing edge increased the strength/downwash of the tip vortices such that the leading-edge vortices were pinned to the wing. Mejia *et al.* (2011) showed similar increases in the lift of a NACA 4415 airfoil at $Re = 900\,000$ using synthetic jet actuation at the trailing edge. In the context of this paper, the downstream blowing/jetting are analogous to decreasing the aspect ratio and the concomitant increase in the influence of the tip-vortex-induced flow facilitates a smooth transition at the trailing edge, thus eliminating or mitigating the generation of trailing-edge vorticity.

6. Topological flow description

In this section we show that, from a topological point of view, the counter-rotating separation region is always present regardless of the particular physical flow configuration, and can be interpreted as a vortex pair. First, we introduce the relation given by Hunt *et al.* (1978) that is satisfied by the critical/fixed points within a two-dimensional plane section of the flow (e.g. the mid-span plane):

$$\left(\sum N + \frac{1}{2}\sum N'\right) - \left(\sum S + \frac{1}{2}\sum S'\right) = 1 - n, \tag{6.1}$$

where N and N' are full and half-nodes, S and S' are full and half-saddles and n is the connectivity of the plane, which is $n = 2$ for the current case; N, N' and S, S' are also recognized as four-way/three-way elliptical and hyperbolic critical points, respectively (Lipinski, Cardwell & Mohseni 2008). In fully attached flow, the only critical points are two half-saddles at the leading and trailing edges. Alternatively, the vorticity can be thought of as entirely confined in the wing as a vortex doublet and each sign of vorticity represents the boundary layers on the wing. The streamlines of a vortex pair are shown in figure 6(*a*), and there are two full nodes and two full saddles.

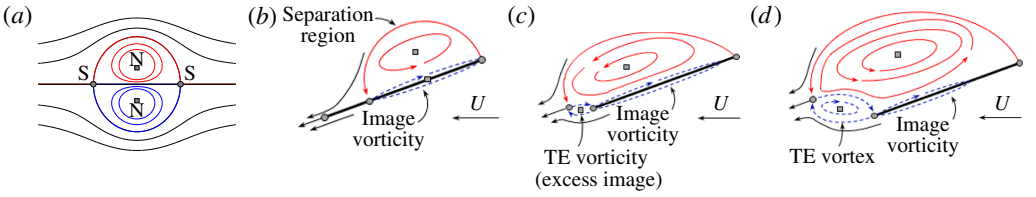

FIGURE 6. (Colour online) (*a*) Streamlines of a vortex pair; grey squares/circles are nodes/saddles. (*b*) Separated, but reattached flow with x_r existing on the wing. The separation region has an image inside the wing. (*c*) Just after x_r has passed the trailing edge and the excess image vorticity has begun to shed into the fluid. (*d*) Fully separated flow, where the forming counter-rotating separation region is fed by the image vorticity. Despite the different physical ramifications of these cases, the vortex structures can be thought of as topologically equivalent.

However, when the body streamline is mapped to the flat-plate wing, the two nodes cancel and the saddles reduce to half-saddles to be consistent with (6.1).

The situation when the flow is separated at the leading edge, but reattaches is shown in figure 6(*b*). The forward and rear stagnation points of the LESR are also half-saddles. Alternatively, the anti-clockwise half of the vortex pair is allowed to enter the fluid as a full node via the leading-edge singularity and represents the LESR; the clockwise half remains confined to the wing as part of the image system. For the time-averaged flows here, the forward stagnation point always coincides with the leading edge and thus a full saddle exists there, consistent with the full saddle of the vortex pair. Up to this point, the mean-flow topology is similar to that described by Rival *et al.* (2014) for the LEV of two-dimensional plunging profiles. However, we observe different characteristics of the mean flow when x_r moves past the trailing edge and into the fluid.

Figure 6(*c*) shows the case when x_r has just passed the trailing edge. The excess image vorticity is shed to create the trailing-edge vortex sheet and the clockwise half of the vortex pair enters the fluid as a full node through the trailing-edge singularity. The flow does not immediately go around the trailing edge, but rather continues along a dividing streamline coincident with the vortex sheet, and so either a full or half-saddle exists at the trailing edge. When x_r goes further beyond the trailing edge (figure 6*d*), the image vorticity is continually fed into the fluid at the trailing-edge singularity and the counter-rotating separation region grows in size. Figure 3 confirms these flow patterns. Now, the CRSR configuration must also be consistent with (6.1). So far, there are two full nodes representing the counter-rotation, and two full saddles at the leading edge and at the rear of the separation region. The recirculating flow of the trailing-edge node connects back to the plate as a half-saddle, and hence there must be a half-saddle at the trailing edge. However, figure 3 indicates that this flow connects back right at the trailing edge so that the two half-saddles merge into a full saddle, which is consistent with the trailing edge as the source of vorticity. Hence, the topology of the flow can always be viewed as a vortex pair with additional half-saddles to account for physical flow separations.

7. Concluding remarks

The mean-flow reattachment of steadily translating low-aspect-ratio wings ($\mathcal{AR} =$ 0.75–2.5) was investigated experimentally with planar DPIV at the mid-span plane.

The chord-based Reynolds number was $Re = 80\,000$ and the angle of attack was ranged from zero to 45° for each wing. Continued lift generation at high incidences is achieved only by wings with $\mathcal{AR} < 1.5$, because reattached mean flow is maintained by the tip vortex downwash, whereas fully separated flow occurs for larger aspect ratios.

The tip-vortex-induced flow facilitates a smooth flow at the trailing edge and therefore helps enforce a Kutta condition there. As a result, the strength of vorticity shed at the trailing edge is decreased, and this consequently results in the continued generation of Joukowski-type lift at high angles of attack for sufficiently low aspect ratios. Just below the static lift-stall angle of attack, strong vorticity is shed at the trailing edge, meaning that the reattachment becomes increasingly intermittent and will lead to large fluctuations in the lift force that are characteristic of incidences near stall. This suggests that with a further increase of incidence or aspect ratio the tip vortex downwash will become even less effective. As such, the intermittent reattachment and eventual fully separated flow will spread across the trailing edge of the wing leading to stall. Hence, the appearance of strong trailing-edge vorticity at mid-span could serve as stall detection.

The flow was also described through concepts consistent with inviscid, potential flow. Reattached flow is characterized by an effective bound circulation around the wing and separation region, resulting in the continued lift generation. When vorticity is shed from the trailing edge, the effective bound circulation is decreased, leading to lift stall. These statements were confirmed with the experimental measurements of mid-span circulation. Lastly, the flow was described with a topological analysis. The mean-flow topology can be interpreted as a vortex pair with 0, 1 and 2 additional half-saddles representing the attached, reattached and fully separated physical flow configurations, respectively.

The exact angle of attack and value of the aspect ratio for which the flow can be reattached at high incidences is also dependent on the Reynolds number, meaning the reattachment process can be assisted by transition to turbulence in the leading-edge shear layer. Nonetheless, we believe that the general progression of the vortex topology as described in this paper can be extended or generalized to other flow regimes. Reynolds number effects as well as different planform and leading-edge geometries are ideal subjects for future work in this area. Also important is the unsteady vortex shedding and its connection to the instantaneous aerodynamic loads on low-$\mathcal{AR}$ wings and is a topic currently under investigation by the authors.

Acknowledgements

This work was supported by the Air Force Office of Scientific Research (AFOSR). The authors wish to thank the anonymous reviewers whose comments greatly helped improve the impact of this manuscript.

REFERENCES

AIAA STANDARDS 2003 Calibration and use of internal strain-gage balances with application to wind tunnel testing. *Report* AIAA Recommended Practice R-091-2003.

BATCHELOR, G. K. 1956 A proposal concerning laminar wakes behind bluff bodies at large Reynolds number. *J. Fluid Mech.* **1**, 388–398.

BERNAL, L. P. 2016 Unsteady aerodynamics of pitching low-aspect-ratio wings: a review of AVT 202 panel results (invited paper). In *Proceedings of the 54th AIAA Aerospace Sciences Meeting (San Diego, CA, USA)*, pp. 1–17.

BIRCH, J. M. & DICKINSON, M. H. 2001 Spanwise flow and the attachment of the leading-edge vortex on insect wings. *Nature* **412** (6848), 729–733.

CARR, Z. R., DEVORIA, A. C. & RINGUETTE, M. J. 2015 Aspect-ratio effects on rotating wings: circulation and forces. *J. Fluid Mech.* **767**, 497–525.

CLARK, R. W., SMITH, J. H. B. & THOMPSON, C. W. 1975 Some series expansion solutions for slender wings with leading-edge separation. *Report* ARC R&M 3785. Ministry of Defence, London, UK.

DEVORIA, A. C. & MOHSENI, K. 2015 Vortex structure of low-aspect-ratio wings in sideslip. In *Proceedings of the AIAA Aerospace Sciences Meeting (Kissimmee, FL, USA)*.

DEVORIA, A. C. & RINGUETTE, M. J. 2012 Vortex formation and saturation for low-aspect-ratio rotating flat-plate fins. *Exp. Fluids* **52** (2), 441–462.

DICKINSON, M. H. & GOTZ, K. G. 1993 Unsteady aerodynamic performance of model wings at low Reynolds numbers. *J. Expl Biol.* **174**, 45–64.

ELDREDGE, J. D., WANG, C. & OL, M. 2009 A computational study of a cononical pitch-up, pitch-down wing maneuver. In *Proceedings of the 39th AIAA Fluid Dynamics Conference (San Antonia, TX, USA)*, pp. 1–14.

ELLINGTON, C. P., VAN DEN BERG, C., WILLMOTT, A. P. & THOMAS, A. L. R. 1996 Leading-edge vortices in insect flight. *Nature* **384** (6610), 626–630.

GARMANN, D. J. & VISBAL, M. R. 2014 Dynamics of revolving wings for various aspect ratios. *J. Fluid Mech.* **748**, 932–956.

GOLDSTEIN, S. 1938 *Modern Developments in Fluid Dynamics, Volumes 1 & 2*, 1st edn. Oxford University Press.

HUNT, J. C. R., ABELL, C. J., PETERKA, J. A. & WOO, H. 1978 Kinematical studies of the flows around free or surface-mounted obstacles; applying topology to flow visualization. *J. Fluid Mech.* **86**, 179–200.

JARDIN, T., FARCY, A. & DAVID, L. 2012 Three-dimensional effects in hovering flapping flight. *J. Fluid Mech.* **702**, 102–125.

JIAN, T. & KE-QIN, Z. 2004 Numerical and experimental study of flow structure of low-aspect-ratio wings. *J. Aircraft* **41**, 1196–1201.

KAPLAN, S. M., ALTMAN, A. & OL, M. 2007 Wake vorticity measurements for low-aspect-ratio wings at low Reynolds number. *J. Aircraft* **44**, 241–251.

KATZ, J. 1981 A discrete vortex method for the non-steady separated flow over an airfoil. *J. Fluid Mech.* **102**, 315–328.

KIM, D. & GHARIB, M. 2010 Experimental study of three-dimensional vortex structures in translating and rotating plates. *Exp. Fluids* **49**, 329–339.

KOOCHESFAHANI, M. 1989 Vortical patterns in the wake of an oscillating airfoil. *AIAA J.* **27** (9), 1200–1205.

LIGHTHILL, M. J. 1973 On the Weis–Fogh mechanism of lift generation. *J. Fluid Mech.* **60** (1), 1–17.

LIPINSKI, D., CARDWELL, B. & MOHSENI, K. 2008 A Lagrangian analysis of a two-dimensional airfoil with vortex shedding. *J. Phys.* A **41** (34), 344011.

MANCINI, P., MANAR, F., GRANLUND, K., OL, M. & JONES, A. R. 2015 Unsteady aerodynamic characteristics of a translating rigid wing at low Reynolds number. *Phys. Fluids* **27**, 123102.

MAXWORTHY, T. 1979 Experiments on the Weis–Fogh mechanism of lift generation by insects in hovering flight. *J. Fluid Mech.* **93** (1), 47–53.

MCCROSKEY, W. J. 1982 Unsteady airfoils. *Annu. Rev. Fluid Mech.* **14**, 285–311.

MEJIA, O. D. L., MOSER, R. D., BRZOZOWSKI, D. P. & GLEZER, A. 2011 Effects of trailing-edge synthetic jet actuation of an airfoil. *AIAA J.* **49** (8), 1763–1777.

OL, M. & BABINSKY, H. 2016 Unsteady flat plates: a cursory review of AVT-202 research (invited). In *Proceedings of the 54th AIAA Aerospace Sciences Meeting (San Diego, CA, USA)*, pp. 1–17.

OL, M. V., BERNAL, L., KANG, C.-K. & SHYY, W. 2009 Shallow and deep dynamic stall for flapping low Reynolds number airfoils. *Exp. Fluids* **46**, 883–901.

OZEN, C. & ROCKWELL, D. 2012 Three-dimensional vortex structure on a rotating wing. *J. Fluid Mech.* **707**, 541–550.

PITT FORD, C. W. & BABINSKY, H. 2013 Lift and the leading-edge vortex. *J. Fluid Mech.* **720**, 280–313.

POLHAMUS, E. C. 1966 A concept of the vortex lift of sharp-edge delta wings based on a leading-edge suction analogy. *Tech. Rep.* TN D-3767. NASA, Langley Research Center, Hampton, Virginia.

RAE, W. H. & POPE, A. 1984 *Low-Speed Wind Tunnel Testing*, 2nd edn. Wiley.

RAFFEL, M., WILLERT, C. E. & KOMPENHANS, J. 1998 *Particle Image Velocimetry*. Springer.

RIVAL, D. E., KRIEGSEIS, J., SCHUAB, P., WIDMANN, A. & TROPEA, C. 2014 Characteristic length scales for vortex detachment on plunging profiles with varying leading-edge geometry. *Exp. Fluids* **55** (1), 1660.

SAFFMAN, P. G. & SHEFFIELD, J. S. 1977 Flow over a wing with an attached free vortex. *Stud. Appl. Maths* **57**, 107–117.

SAFFMAN, P. G. & TANVEER, S. 1984*a* Prandtl-batchelor flow past a flat plate with a forward-facing flap. *J. Fluid Mech.* **143**, 351–365.

SAFFMAN, P. G. & TANVEER, S. 1984*b* Vortex induced lift on two dimensional low speed wings. *Stud. Appl. Maths* **71**, 65–78.

SHIELDS, M. & MOHSENI, K. 2013 Roll stall for low-aspect-ratio wings. *J. Aircraft* **50** (4), 1060–1069.

SHYY, W., TRIZILA, P., KANG, C.-K. & AONO, H. 2009 Can tip vortices enhance lift of a flapping wing? *AIAA J.* **47** (2), 289–293.

TAIRA, K. & COLONIUS, T. 2009*a* Effect of tip vortices in low-Reynolds-number poststall flow control. *AIAA J.* **47** (3), 187–207.

TAIRA, K. & COLONIUS, T. 2009*b* Three-dimensional flows around low-aspect-ratio flat-plate wings at low Reynolds numbers. *J. Fluid Mech.* **623**, 187–207.

VISBAL, M., YILMAZ, T. O. & ROCKWELL, D. 2013 Three-dimensional vortex formation on a heaving low-aspect-ratio wing: computations and experiments. *J. Fluids Struct.* **38**, 58–76.

WEIS-FOGH, T. 1973 Quick estimates of flight fitness in hovering animals, including novel mechanisms for lift production. *J. Expl Biol.* **59**, 169–230.

WINTER, H. 1936 Flow phenomena on plates and airfoils of short span. *Tech. Mem.* 798. National Advisory Committee for Aeronautics.

WOJCIK, C. J. & BUCCHOLZ, J. H. J. 2014 Vorticity transport in the leading-edge vortex on a rotating blade. *J. Fluid Mech.* **743**, 249–261.

XIA, X. & MOHSENI, K. 2013 Lift evaluation of a two-dimensional pitching flat plate. *Phys. Fluids* **25** (9), 091901.

XIA, X. & MOHSENI, K. 2016 Unsteady aerodynamics and trailing-edge vortex sheet of an airfoil. In *Proceedings of the AIAA Aerospace Sciences Meeting (San Diego, CA, USA)*.

YILMAZ, T. O. & ROCKWELL, D. 2012 Flow structure on finite-span wings due to pitch-up motion. *J. Fluid Mech.* **691**, 518–545.